



HAL
open science

Chapter Six - Strategies for crystallization of natural ribozymes

Benoit Masquida, D Sibrikova, Maria Costa

► **To cite this version:**

Benoit Masquida, D Sibrikova, Maria Costa. Chapter Six - Strategies for crystallization of natural ribozymes. Ribozymes, Wiley-VCH, 2020, 10.1002/9783527814527.ch30 . hal-03002014

HAL Id: hal-03002014

<https://hal.science/hal-03002014v1>

Submitted on 12 Nov 2020

HAL is a multi-disciplinary open access archive for the deposit and dissemination of scientific research documents, whether they are published or not. The documents may come from teaching and research institutions in France or abroad, or from public or private research centers.

L'archive ouverte pluridisciplinaire **HAL**, est destinée au dépôt et à la diffusion de documents scientifiques de niveau recherche, publiés ou non, émanant des établissements d'enseignement et de recherche français ou étrangers, des laboratoires publics ou privés.

6.2 Strategies for crystallization of natural ribozymes

B. Masquida*, D. Sibrikova, Maria Costa

6.2.1 Introduction

The group of ribozymes acting like turnover enzymes is up to now restricted to the ribonuclease P [1], the ribosome [2] and the spliceosome [3]. Other natural ribozymes are endonucleolytic RNAs, catalyzing the reversible cleavage of a phosphodiester bond within their own chain. This group contains the hammerhead [4], hairpin [5], hepatitis delta virus (HdV) [6], and the Varkud satellite (VS) [7] ribozymes, and also group I [8, 9] and group II introns [9]. More recently discovered ribozymes include twister [10], twister sister, pistol and hatchet [11], as well as GlmS [12], which is also a riboswitch. When the cleavage intervenes at the boundaries of the ribozyme, like in the case of the HdV ribozyme, the structure of the initial, or pre-catalytic RNA is expected to be quite similar to the 3' cleavage product. Yet, most frequently, cleavage intervenes at an internal position. In the course of the reaction, the amount of pre-cleavage form decreases in solution until the catalytic equilibrium is reached. As fragments of the ribozyme itself, the RNA cleavage products may not be able to fold properly since cleavage affects the higher order structure of the RNA by splitting structural domains. Therefore, a solution of active ribozymes ends up as a mix of different characteristic RNA precursors and products, to which should be added shorter species resulting from the degradation of unstable cleavage products.

Crystallization of biomolecules requires chemical and conformational homogeneity [13]. RNA incubation in crystallization droplets usually lasts a couple of days or weeks at temperatures ranging from 15°C to 37°C, at pH comprised between 6 to 8, in the presence of monovalent and divalent and/or trivalent ions, like magnesium salts or

coordinated transition metals such as cobalt, osmium or iridium that serve solving the phase problem using anomalous diffraction or scattering methods. Lanthanides can also be used for this purpose. Apart from crystallization agents such as ammonium sulphate, oily alcohols (MPD) or polyethylene glycols (PEG) of different molecular weights, various additives such as polyamines (spermine, spermidine) can be used. Even though not optimal, these conditions allow for some ribozyme activity, meaning that pre- and post-cleavage forms of the ribozyme may co-exist in the sample before the crystallization occurs. Preventing ribozymes to catalyze their own reaction is thus a mandatory aspect of ribozyme structural biology that requires designing unreactive constructs, yet still able to fold into the catalytically relevant conformation.

Endonucleolytic ribozymes catalyze RNA cleavage through a phosphodiester transesterification pathway based on the exchange of two phosphodiester bonds. The conservation of energy storage in this reaction allows for its reversibility. The reaction consists in a nucleophilic attack promoted by the 2'-hydroxyl group adjacent to the reactive phosphate group and generates 2',3'-cyclic phosphate and 5'-hydroxyl product termini. This 2'-OH group needs to be activated to become an efficient nucleophile to attack the 3'-adjacent phosphate group. However, the reaction relies on additional chemical and structural requirements. Going stepwise from activation to product formation, the catalytic pathway consists of successive chemical and conformational steps. Structural biologists need to find strategies to block the ribozymes under scrutiny at a single step in order to isolate conformers corresponding to a well-defined state along the catalytic pathway. As a general rule, success stems from good knowledge of the ribozyme catalytic behavior deduced from biochemical studies prior to the design of the RNA constructs, which will be assayed for crystallization. Several strategies can be employed to prevent the reaction to occur. This chapter reviews these strategies and

illustrates them with representative examples of natural small ribozymes and self-splicing introns.

6.2.2 Strategies to inactivate the nucleophile

Endonucleolytic ribozymes exhibit different chemical properties (exhaustively summarized in [14]) to become efficient catalysts. In brief, the phosphodiester transesterification reaction consists in a bimolecular nucleophilic substitution (S_N2). The S_N2 -like reaction is characterized by the formation of the new bond, generating a pentavalent phosphorous intermediate, followed by cleavage of the leaving group, a mechanism that energetically culminates with the formation of a phosphorane transition state. This situation leads to chirality inversion if the atom targeted by the nucleophile is asymmetric. The transesterification mechanism assumes that the nucleophilic hydroxyl group is activated by deprotonation following action of a general base. The structure of the ribozyme provides an architecture that favors the placement of the nucleophile in line with the phosphorus and leaving 5'-oxygen atom. The alignment of these three atoms is required for the formation of the pentavalent phosphorane transition state, which adopts a trigonal bi-pyramidal geometry. The transition state needs also to be stabilized structurally by the ribozyme architecture, notably through an increased number of H-bonds. Finally, the leaving oxyanion should be stabilized by an acid, which gives a proton to stabilize the conjugated base, the 5'-hydroxyl. This catalytic mechanism is very much similar to the one operated by the RNase A enzyme, in which all the above-mentioned atoms are aligned to perform the S_N2 -like reaction [15]. All these steps add on individually to result in the final catalytic

rate. Vice-versa, disturbance of any of these steps decreases the overall reaction rate. In principle, the modification of the chemical groups involved in any of these events can help decrease the overall catalytic rate sufficiently to render the ribozyme inactive enough over the incubation time necessary for crystallization. The most straightforward strategy is to remove or replace the nucleophilic oxygen atom by molecular engineering. Another strategy consists in mutating the residues that will either activate the nucleophile or stabilize the leaving group. Finally, the scissile phosphate group can be omitted by synthesis of split oligonucleotides or by circular permutation.

Another critical aspect regarding ribozymes crystallization is related to the integrity of their architecture. The 5'- and 3'-boundaries of ribozymes are not always easy to define. Moreover, loops can contain additional domains dispensable for the ribozyme catalytic architecture. Usually, efforts are made to reduce the length of the ribozyme constructs while retaining significant catalytic activity. This strategy can lead to the removal of regions that are somewhat dispensable for the catalysis but critical for the architecture. Nevertheless, some domains may also confer to the ribozymes too much flexibility, which may prevent folding as a single conformation. In these cases, adequate domain replacement monitored by conformational analysis can help improve the situation. Illustrations of these situations will be given in the paragraphs below.

6.2.3 When the cleavage site is at the edge of the ribozyme

The location of the cleavage site at the 5'-boundary of the ribozyme constitutes the most ideal situation, since the 3'-RNA product corresponds to the entire ribozyme domain and

the other one to a dispensable short fragment. The cases of the hepatitis delta (HdV, [16]) and of the GlnS [17, 18] ribozymes well illustrate this situation, where the ribozyme domains are located downstream from the cleavage site. The cleavage product corresponding to the ribozyme core can be purified from an in vitro cleavage assay. Yet, the study of the catalytic mechanism requires the presence of the scissile nucleotide. The latter can be added by hybridization of a ribozyme domain made from an oligonucleotide mimicking the unreacted substrate by bearing a specific chemical modification inhibiting catalysis.

When the structure of the HdV ribozyme [16, 19] was solved (Figure 6.2.1), the only RNA structures that were known apart from a variety of helical structures, were of tRNAs [20, 21], of two versions of the hammerhead ribozymes [22, 23], and of the P4-P6 domain from the *Tetrahymena* intron [24]. In this context, the main goal was to expand the RNA structural repertoire by solving the structure of a new RNA architecture. When embedded in a viroid, the ribozyme allows to cleave the multimeric RNA copy resulting from the viroid RNA replication through a rolling circle mechanism into individual genomes and simultaneously to ligate their ends to form circles [25]. In spite of the absence of sequence requirements and of need for catalytic ions, the 5'-hydroxyl cleavage product of the ribozyme was purified to sort out the misfolded intermediates and meet the chemical and conformational homogeneity of the sample required for crystallization. Among the structural features unraveled by the first crystal structure of the HdV ribozyme [16], a pseudoknot (P1.1) formed by two consecutive G=C base pairs was observed between residues from loop L3 and the junction of stems P1 and P4 (J1/4), in addition to the one already known from comparative sequence analysis that leads to the formation of the P2 stem. P1.1 is actually instrumental for positioning the first residue of the ribozyme 3'-cleavage product, G+1, which is involved in a wobble

pair with U37. Residue C75 has been identified as the residue responsible for the limiting proton transfer step of the catalytic reaction. C75 should either abstract the proton of the 2'-hydroxyl of U-1 [26, 27] or stabilize the 5'-oxyanion of the leaving group [28]. In agreement with these data, the crystal structure shows that the N3 Watson-Crick group of C75 establishes a hydrogen bond with the 5'-hydroxyl group of G1. However, this property would imply that the pKa of C75(N3) were was around ~7 instead of 4.2 as observed for the free cytosine. This hypothesis was addressed by NMR, and only a weak increase of the pKa was observed in the context of the HdV cleavage product [29]. Further crystallographic studies were carried out to investigate the structure of the pre-cleavage form of the ribozyme. Catalysis was prevented in these constructs following strategies that will be presented below.

The GlmS RNA is a ribozyme and also a riboswitch that binds glucosamine-6-phosphate (GlcN6P), a bacterial and fungal cell wall precursor [30]. The cellular concentration of GlcN6P negatively controls the RNA amount of *glms*, the gene producing the GlcN6P synthase [12]. While several crystal structures of the aptamer domain of this riboswitch have been solved, the folding energetic landscape between the GlcN6P bound and unbound conformations of the riboswitch have only been investigated recently [31]. The first structural study from the *Thermoanaerobacter tengcongensis* GlmS constructs gathered crystal structures with or without the scissile residue allowing comparison between the conformations of the pre- and post-cleavage forms [17, 32]. Yet, the binding of glucose-6-phosphate (Glc6P), an inhibitor of the GlmS riboswitch, but not of GlcN6P could be observed. Only models of the catalytic mechanism could be deduced from these structures. Just after reporting the crystal structure of the *T. tengcongensis* GlmS riboswitch, another research group published the crystal structure of the *Bacillus anthracis* GlmS riboswitch in the presence of the ligand (Figure 6.2.2b). The direct

involvement of the amino group of GlcN6P to protonate the leaving 5'-oxyanion during catalysis could be demonstrated [18].

This set of crystal structures shows that when cleavage intervenes at the 5'-end, the addition of a couple of 5'-nucleotides does not have major effects on the overall ribozyme architecture. However the addition of 5'-nucleotides restores the cleavage site, requiring inhibition of the nucleophile activation. Strategies used to prevent nucleophile activation are described below.

6.2.4 Removal or neutralization of the catalytic 2'-hydroxyl group

With a lesser knowledge of the catalytic mechanism, meaning when the nucleophile position has been identified, but not much other informations are available, the easiest strategy is either to remove the 2'-hydroxyl group or to modify it by methylation.

Removal may lead to a loss of information by releasing some of the constraints on the active nucleotide, while methylation preserves the 2'-O-atom, which potentially confers the opportunity to observe its role in catalysis.

6.2.4.1 The hammerhead ribozyme

The hammerhead ribozyme was the first catalytic RNA, the structure of which was solved by crystallography [22]. The ~50 nt hammerhead ribozyme was found in the 80's in the satellite RNA of the avocado sunblotch viroid [4]. More recently, genome surveys have revealed that the hammerhead motif is actually widespread in genomes, from

bacteria to humans [33]. This fairly short RNA allowed for defining a trans-acting construct based on the hybridization of a ribozyme domain and a substrate strand [34, 35] that acts like a true enzyme/substrate complex.

In the first hammerhead crystal structure, a minimal ribozyme domain was produced by *in vitro* transcription, whereas the substrate strand was chemically synthesized as a DNA strand. This strategy allowed for the systematic replacement of all 2'-hydroxyl groups of the substrate strand by hydrogen atoms and consequently, prevented cleavage at the scissile phosphate. Since the RNA strand geometry cannot fold like B-DNA due to the presence of the 2'-hydroxyl groups, the DNA strand was forced to adopt the A-form [22]. In the structure of the all-RNA hammerhead ribozyme published shortly afterward, a two strands strategy to reconstitute the minimal ribozyme was again chosen. In this case, the nucleotide bearing the proton of the nucleophilic 2'-hydroxyl group was changed to a 2'-*O*-methyl group to block catalysis [23]. In order to impair catalysis during crystallization, neutralization of the nucleophile by chemical modification is preferred over the depletion of the attacking 2'-hydroxyl group. This is because the former strategy is more likely to provide relevant insight into the catalytic mechanism. However, introduction of such chemical modifications relies on solid-phase chemical synthesis (See [36, 37] for Review) of short RNA oligonucleotides carrying the desired modified nucleotides. Indeed, the all-RNA hammerhead ribozyme showed the same conformation as the DNA-RNA hybrid construct. Yet, in both crystal structures, the conformation of the active site was not in agreement with the biochemical and enzymatic data previously obtained for the ribozyme. Also, in these structures, the conformation at the cleavage site did not show the expected alignment of the three atoms involved in the transesterification reaction (Figure 6.2.3a), namely the 2'-hydroxyl of the catalytic residue on one side, and the phosphorus atom and the 5'-

hydroxyl groups of the contiguous 3'-residue on the other side. Subsequently, intensive research was conducted using the minimal RNA construct to try to observe its active conformation by freeze-trapping an active version of the ribozyme at low pH in the presence of magnesium ions [38]. But again, the conformation trapped in the crystal was still not fully supportive of an in-line S_N2 -like mechanism for the self-cleavage reaction. The answer actually came 10 years later when the crystal structure of a longer hammerhead ribozyme derived from *Schistosoma mansoni* was solved (Figure 6.2.3b). This hammerhead ribozyme version comprises additional critical tertiary contacts between peripheral segments that improve catalysis by 1000-fold at sub-millimolar magnesium concentration [39, 40]. For crystallization purposes, a two-strand construct was also used to reconstitute the ribozyme and the nucleophilic 2'-hydroxyl group was again neutralized by methylation. The resulting crystal structure revealed that the active site of this longer ribozyme forms a 3-way junction. Stem II is closed by an apical loop, which interacts with the internal loop embedded in stem I, itself formed between the ribozyme and the substrate strand [41]. This peripheral tertiary interaction induces a major conformational change in the distal 3-way junction that forces the in-line positioning of the three atomic groups involved in the catalytic reaction. The right panel of Figure 6.2.3 shows the very different positions adopted by the dinucleotide around the scissile bond. Taken together, these observations indicate that the historical hammerhead construct that was used as a model system for a long time despite its poor activity had in fact been too much shortened to keep the relevant pre-catalytic conformation [42]. In conclusion, designing a streamline version of a ribozyme for crystallization purposes should rely, first on careful sequence analysis of the available ribozyme variants and, second on careful biochemical and kinetic analysis of each

construct in order to select the molecule that more closely mimics the natural full-length version.

6.2.4.2 Group I intron

The ~300 nt group I ribozymes are able to self-splice along a two-step transesterification mechanism. First, an exogenic guanosine (exoG) binds a pocket in the catalytic core to play the role of the nucleophile. During the first step, exoG transesterifies the bond between the 5'-exon and the intron and remains attached to the 5'-end of the intron. Following a profound conformational change leading to the replacement of exoG by the ultimate G residue (ω G) of the intron in its pocket, the 3'-residue of the 5'-exon cleaves the bond between the intron and the 3'-exon (Figure 6.2.4a). This pathway results in exon ligation and intron release. Capturing intermediates along this complex pathway requires inactivation of well-chosen residues (Figure 6.2.4b, c).

The self-splicing group I intron from the pre-tRNA^{Ile} of bacterium *Azoarcus* [43, 44], was crystallized bound to its exons in a conformation preceding the second catalytic step of splicing. This intron/exons complex was stabilized by four specific 2'-deoxy substitutions: two at intron positions A205 and ω G, one at the end of the 5'-exon and a fourth one at the beginning of the 3'-exon. Collectively, these modifications slow down exon ligation by a million-fold and allow for crystal nucleation and growth over ~2 weeks. The crystallization construct was obtained by hybridization of a transcript corresponding to the majority of the intron with an RNA-DNA oligonucleotide spanning the 3'-section of the intron and the beginning of the 3'-exon, and a trinucleotide

mimicking a short 5'-exon ending with a dT residue. This three-piece strategy greatly facilitated introduction of the substitutions since all of the 2'-deoxy nucleotides were inserted during chemical synthesis of the RNA-DNA chimeric oligonucleotides (Figure 6.2.4). In addition, a U1A binding site was introduced in the L6 loop of the intron to optimize crystallization by promoting crystal packing interactions between molecules in solution [45]. Note that U1A contains Seleno-methionine residues used to solve the phase problem without performing heavy atom soaking or co-crystallization.

The crystallized intron/exons complex revealed the structural basis for 5'- and 3'-splice site selection and substrate alignment used by group I intron ribozymes. However, positioning of the metal ions into the active site was found not to be fully consistent with available biochemical data presumably because of the 2'-deoxy substitution at the terminal intron guanosine ω G [43]. Indeed, only subsequent crystallization of an all-ribose version of the same construct, containing the catalytically essential ω G O2'-ligand, allowed the correct positioning of the metal ions in the active site and provided crystallographic evidence for the 'two-metal-ion' mechanism of group I intron splicing [46]. In this case the same 5'-exon (CAT) trimer was used to reduce sufficiently the exon ligation reaction and permit crystal nucleation. Again, this example nicely illustrates that crystallization of complete ribozymes in their active state is a challenging task: modification of catalytically important positions is necessary to block or reduce the activity of the ribozyme, still, such changes should not alter the catalytically competent structure of the active site.

Other structures of group I introns have been solved by X-ray crystallography [47, 48]. Yet, their conformations did not represent any active state, and thus did not require introduction of any chemical modification. In the structure of the *Tetrahymena* ribozyme [47], the substrate helix was not included in the construct. In the ribozyme of the *orf142*

from the phage Twort [48], the ribozyme core was crystallized with a tetrameric RNA mimicking the substrate. However, since this pseudo-substrate does not correspond to any catalytic step, proper docking onto the ribozyme core could not be observed.

6.2.4.3 Group II intron

Group II introns, which are not evolutionarily related to group I introns, constitute the second class of self-splicing ribozymes known to date. They are abundant in bacteria and bacterial-derived organelles of fungi, plants and algae. Group II introns are large catalytic RNAs of ~600 nucleotides which, in association with the reverse transcriptase they encode, can also behave as mobile retrotransposable elements. Despite their bacterial origin, it is now widely believed that group II introns played a determinant part in eukaryotic evolution as the ancestors of the nuclear pre-messenger introns and their splicing machinery (the spliceosome) [49]. This evolutionary hypothesis is grounded on the extensive structural and mechanistic similarities shared by the two splicing systems. Both group II intron and nuclear pre-mRNA splicing proceed through two sequential transesterification reactions and generate a typical intron form called the 'lariat' intron. Self-splicing of group II introns is initiated by the 2'-hydroxyl group of a highly conserved adenosine, lying unpaired in domain VI (bpA in Figure 6.2.5a), which undergoes a nucleophilic attack at the 5'-splice site. This first splicing step results in the formation of a specific branched intron intermediate, the 'lariat' intermediate, in which the 'branchpoint' adenosine (bpA) becomes covalently linked to the first intron nucleotide, a conserved guanosine, through a 2',5'-phosphodiester bond. It follows the second transesterification reaction, during which the 3'-OH of the cleaved 5'-exon

attacks the 3'-splice site, resulting in the ligation of the flanking exons and the release of the intron 'lariat'. Because transesterification reactions are chemically reversible, excised group II lariats are then able to invade specific RNA or DNA targets by catalyzing the splicing reactions in the reverse order and orientation: this 'reverse splicing' pathway plays an essential role in the biological activities of group II introns, since reverse splicing into DNA triggers the genomic mobility of the intron.

Recent X-ray crystal structures of an excised group II intron lariat, alone or bound to its 5'-exon substrate (Figure 6.2.5), uncovered the structural basis for reverse splicing by group II introns [50]. These structures revealed for the first time that the 2'(A)-5'(G) branch plays a direct and crucial role in organizing the active site for the second step of splicing. Remarkably, the structures also show that after completion of the splicing reaction, the last nucleotide of the freed intron lariat remains firmly positioned in the catalytic center with its 3'-OH activated by a highly coordinated metal ion (M1 in Figure 6.2.5c) and poised for catalysis of the reverse splicing reaction. In the absence of its 5' - and 3'-exon substrates, the excised group II lariat is a stable RNA, therefore, the purified lariat sample could be crystallized without any modification. Formation of a stable lariat/5'-exon complex, however, required co-crystallization of the lariat with an unreactive analog of the 5'-exon. This analog consisted of a 7-mer RNA carrying a 3'-deoxy ribose at its 3'-end (Figure 6.2.5a, c). Removal of the terminal 3'-hydroxyl group of the 5'-exon was necessary to block lariat 'debranching': a reaction that is mechanistically analogous to the reverse of the first step of splicing and, accordingly, leads to the production of linear intron molecules covalently attached to the 5'-exon. Comparison of the lariat structures with and without this substrate revealed that binding of the 5'-exon drives a local conformational rearrangement of domain V that extends into the active site and contributes to coordination of a second catalytic metal ion. Interestingly, native

crystals (grown in magnesium-containing solutions) lacked electron density corresponding to this second metal ion, most probably due to the absence of the critical 3'-OH group of the 5'-exon. Evidence for this second catalytic metal ion was nevertheless obtained through crystal soaking in ytterbium - an anomalous scatterer lanthanide that mimics highly coordinated magnesium ions, but binds with higher affinity. Indeed, ytterbium soakings revealed the presence of two metal ions in the reaction center (Y1 and Y2 in Figure 6.2.5c), one of which perfectly superimposes with metal ion M1 already identified in the native crystals. Altogether, the two sets of crystals allowed the direct observation of all but three metal ion coordinations that build-up the 'two-metal ion' transition state for the reverse splicing reaction (Figure 6.2.5c; [50]). Importantly, the transition state model derived from this crystallographic work is identical to the one prevailing for group I intron self-splicing (see previous section; [46]).

6.2.4.4 The hairpin ribozyme

The hairpin ribozyme provides another example where the precise definition of the domains important for folding was critical to solve a catalytically relevant structure. Like the hammerhead and HdV ribozymes, the hairpin ribozyme is part of the satellite RNA of a virus (tobacco ringspot virus), and chops the multimeric RNA resulting from a rolling circle amplification [5]. The hairpin ribozyme was named after the shape of the secondary structure of the minimal fragment initially studied (Figure 6.2.6). This construct consists in two helical domains (A and B), each incorporating an internal loop [51]. In the initially characterized hairpin ribozyme construct, a kink between domains A and B promotes docking of the internal loops so that catalysis occurs. However,

structural studies in solution have shown that the linker between the domains is very flexible [52, 53]. Closer analysis of the natural structural context indicated that the ribozyme actually folded from a four way junction, bringing into play two additional helices that stack on top of domains A and B in order to form an RNA holiday-like junction [54]. These junctions, like the related DNA holiday junctions instrumental in genomic recombination events [55], form an "X" with each branch corresponding to an helix.

The 5'-helices of domains A and B are tethered so that a kink between them results in docking of internal loops A and B. In a minimal construct presenting only domains A and B, this situation results in high conformational heterogeneity due to constant competition between helical stacking at the edge of the two domains and docking of the internal loops. FRET experiments indicated that upon folding, the natural 4-way junction was forming a dominant conformation forcing the two domains required for catalysis to dock productively. The 4-way junction context thus increases dramatically the rate of interaction between domains A and B as compared to the original and much more flexible hairpin construct corresponding to the minimal construct [52]. This 4-way junction hairpin ribozyme RNA to which a U1A protein binding site was added to improve crystallization [45] was finally solved by X-ray crystallography [56]. Like in the case of the all-RNA hammerhead ribozyme, the nucleophilic 2'-hydroxyl group from the substrate strand was neutralized by methylation. The structure showed close to perfect alignment between the three atoms involved in the S_N2 -like reaction as well as pointed to a network of hydrogen bonds stabilizing the pre-catalytic state. In particular, the scissile G residue is pulled out from domain A by forming a trans Watson-Crick base pair with an unpaired C of domain B, which orients its backbone favorably for the S_N2 -like reaction (Figure 6.2.6d). It is worth to note that the structure of an all-RNA substrate

hairpin ribozyme could be solved despite its catalytic activity. In this case, the constraints from the crystal packing together with the occurrence of the ligation reaction seem to prevent product strands dissociation [57].

In order to go beyond the structure of the ground state and to elucidate the catalytic mechanism, another modification strategy of the ribozyme was undertaken to study the structure of the transition state. This strategy relies on the coordination of both the 2' - and 3'-hydroxyl groups of the residue bearing the nucleophile and of the 5'-hydroxyl group of the downstream nucleotide by a vanadate ion. Vanadate coordination fairly well mimics the phosphorane intermediate generated during the cleavage reaction [57]. To allow binding of the vanadate ion, the substrate was split into two fragments resembling the reaction products with free 2', 3'- and 5'-hydroxyl groups. This strategy leads to the removal of the scissile phosphate, which is replaced by the vanadate ion. The crystal structure reveals how the transition state is stabilized throughout increasing the number of hydrogen bonds formed with the two nucleotides in the vicinity of the vanadate (Figure 6.2.6e). Noteworthy, the structure of the ribozyme with a split substrate displaying a 2',3'-cyclic phosphate at the cleavage site could also be solved to complete the snapshots necessary to describe the entire catalytic process [57]. The structure of the transition state of the hammerhead ribozyme was also studied using vanadate ion binding to the cleavage site [58, 59]. The catalytic site undertakes a substantial reshaping under these conditions and allows for describing more accurately the role of the residues and ions potentially involved in the reaction, notably G12, the general base, and the two magnesium ions close to the scissile bond. The vanadate structure also suggests that a water molecule bound to a divalent cation could act as the general acid that stabilizes the 5' oxy-anion.

6.2.5 Removal of the scissile phosphodiester bond using circular permutation

Success of the split substrate strategy relies on efficient hybridization of the RNA strands to their target as in the case of the hairpin ribozyme. However, this pre-requisite is not always met since annealing efficiency depends on the length and concentration of three different RNA species, each one potentially engaged in individual folding events that might perturb the formation of a well-folded trimer. Moreover, if the substrate binds to a region with an intricate fold, hybridization itself may be inefficient. An example that illustrates this situation is given with the lariat capping ribozyme (LC) [60], which is the topic of an entire chapter in the present book (Chapter X). In brief, this ribozyme catalyzes a transesterification reaction called 'branching' that is initiated by the nucleophilic attack of a 2'-hydroxyl group from a U residue on a C residue residing two nucleotides upstream. This reaction leads to the formation of a short 3 nt lariat in which the U residue is covalently attached to the C residue through a 2',5'-phosphodiester bond [61]. From a chemical point of view, the lariat is identical to those generated by group II introns and the spliceosome during the first step of splicing [3], except that the lariat loops involved in splicing span hundreds of nucleotides instead. In the case of the LC ribozyme, the 2',5'-branch point structure is well buried into the ribozyme core, where each nucleotide from the lariat weaves specific stacking and hydrogen bond interactions with specific core residues. These non-canonical interactions could not be deduced from comparative sequence analysis since the lariat sequence is fully conserved among all LC ribozyme homologues [62]. Most importantly, the sequence stretch 3' from the cleavage site directly contributes building up the 3-way junction of the regulatory domain, which works by forming a receptor for a residue

within a loop of the ribozyme core, instrumental for structuring the catalytic site. Initial efforts to crystallize the ribozyme using synthetic oligonucleotides were unsuccessful, because the hybrids could not properly fold.

To overcome this problem, a circular permutation strategy was implemented to swap the extremities of the ribozyme to the residues around the scissile phosphodiester, while the natural ends located in the stem were tethered by a UUCG tetraloop [63] (Figure 6.2.7). Without any starting G residues, the 5'-CAU sequence resulting from this permutation did not follow at all the sequence requirements of the enzyme used to produce the RNA in vitro, the T7 RNA polymerase. For production purpose, a 5'-hammerhead ribozyme domain was thus inserted upstream from the LC ribozyme. Since the hammerhead was introduced to increase the transcription yield of the LC ribozyme, the optimal sequence transcribed by the T7 RNA polymerase was introduced right downstream from the T7 promoter [63]. The version of the ribozyme based solely on the 3-way junction proved to be inefficient at cleaving, certainly because the LC ribozyme could fold faster, preventing the hammerhead ribozyme to adopt a structure prone to cleave. Consequently, the hammerhead was optimized for fast-folding by preserving the tertiary contacts observed in the *Schistosoma* ribozyme [40]. In addition, an HdV ribozyme was added at the 3'-end of the LC ribozyme to guarantee that the construct would not present any additional residue after its terminal G, ωG.

The structure of the circularly permuted LC ribozyme allowed to uncover all the interactions that the three lariat residues mediate with the other nucleotides from the core. It is worth noting that a water molecule interacts with the 2'-hydroxyl of U232 and the 5' hydroxyl of C230, and could be considered reminiscent of the scissile phosphate group that is available in the natural LC ribozyme, but missing in the circularly permuted form due to the construct design (Figure 6.2.7). Nevertheless ωG, which is

important for catalytic activity, could not be observed due to structural disorder. This indicates that the conformation captured in the crystal corresponds to a snapshot of the LC ribozyme right after catalysis and before release of the RNA products.

Interestingly, circular permutations intervene naturally in RNA sequences. Domain shuffling can lead to RNA circular permutations, notably in back-splicing events resulting in the appearance of circular RNAs originating from pre-mRNAs [64, 65]. As far as the active RNA structure is maintained, the position of the 5'- and 3'-ends can be located in different regions. Along the same idea, loops closing helices can adopt any length from 3 nt to several kb as far as the few nucleotides contributing to tertiary interactions are preserved, if any. Such examples of natural circularly permuted RNAs have been described for the signal recognition particle (SRP) [66] and for the hammerhead and HdV-like ribozymes [67, 68]. Circular permutations can also be engineered to incorporate chemically modified residues further used in biochemical studies [69-72]. Examples involving ribozymes include the RNase P where circular permutations were engineered to insert photo-agents to perform cross-linking studies [70] or to study folding kinetics [73].

In principle, circular permutation (CP) can be engineered on any RNA, provided that the 5'-sequence follows the requirement of the RNA polymerase that will be used to transcribe it from the DNA template. CP is thus a method of choice to express an RNA as a single molecule, based on the idea that the removal of the scissile phosphate group does not prevent homogenous folding.

6.2.6 Mutation of residues involved in the acido-basic aspects of transesterification

The 154 nt Varkud Satellite (VS) ribozyme is a fairly large ribozyme within the family of nucleolytic ribozymes. It is found in the mitochondria of a specific isolate of the *Neurospora* fungus [7]. Inactivation of the VS ribozyme for crystallization purpose was achieved following an original strategy based on modifying the residues involved in the proton transfer necessary for stabilizing the catalytic intermediates [74]. In brief, its structure is organized around three 3-way junctions encompassing seven helices (numbered 1 to 7). From each of those 3-way junctions protrudes one stem-loop, each one contacting a specific region of the ribozyme (Figure 6.2.8). The stacking between stems from the 3-way junctions generates a helical region spanning four helices (1 to 4). The structure shows a feature so far unique to this ribozyme. The ribozyme crystallizes as a dimer in which the substrate stem (numbered 1) of one ribozyme docks in the second ribozyme in a catalytically active conformation [74]. This conformation is characterized by the formation of a kissing complex between the loops of helices 1 from one ribozyme and the loop from helix 5 of the second. Interestingly, these two 7 nt loops adopt similar conformations reminiscent of the anticodon loop of tRNAs. In each loop, a U-turn intervenes after the second nucleotide allowing the next four ones to adopt a conformation consistent with the formation of a four base pairs helix. In tRNAs, the fourth helical nucleotide is often hyper-modified to avoid decoding mistakes [75]. The *trans* interaction between loops 1 and 5 leads to the docking of the substrate along helices 2 and places the internal loop from helix 6 in position to build up the active site. The observed dimer is in agreement with former biochemical, NMR data, and SAXS structure determination [76].

The strategy implemented by the authors was motivated by obtaining the RNA as a single strand to be able to purify it under native conditions since the dimer formed in the course of the transcription reaction. The structures of two mutants were solved,

each one strongly affecting proton transfer in the catalytic site. The G638A structure was solved by single wavelength anomalous diffraction (SAD), and the A756G structure was solved by the molecular replacement method using the G638A structure as a search model. Residues important for catalysis locate in stems 1 and 6. In helix 1, G638 acts as a general base to abstract the proton of the 2'-hydroxyl group of the cross-strand stacked guanine. Helix 6 harbors A756, the general acid that stabilizes the leaving oxy-anion after the formation of the phosphorane transition state. The two X-ray structure models of the mutant forms G638A and A756G of the VS ribozyme unravel how the two residues contribute both to the structure and to the catalysis.

In the G638A structure, the O2', phosphorus and O5' atoms of the scissile bond between G620 and A621 are not perfectly in line, showing that the mutation significantly affects the activation of the reaction (Figure 6.2.8c). The extrusion of A621 from its helix and further stabilization through A-minor binding to a G=C pair in helix 2 indicate how the in-line positioning of the three atoms taking part in the S_N2 -like reaction may be easily achieved. However, A638, which stacks on the face of G620 points its Watson-Crick edge towards the phosphate group of A621. This situation places N1 of A638 in close enough proximity of the O2'-group from G620 and supports the notion that G638 is the general base involved in activation of the reaction. In the G638A crystal structure, the general acid A756 also points towards the phosphate group of A621. Noteworthy, a water molecule is clamped by hydrogen bonds between N1 of A756 and O2P of A621. The position of this water molecule could mimic the O5'-ligand of the phosphorane intermediate that would be resolved by proton transfer from A756, which would be protonated on its N1 atom (Figure 6.2.8).

In the A756G structure model (Figure 6.2.8d), the three groups involved in the S_N2 -like reaction are placed in-line much better than in the G638A VS ribozyme RNA. Similar to

the G638A crystal structure, A621 is extruded from its helix to make an A-minor contact within the shallow groove of helix 2. The distance between the O2'-nucleophile and the N1 group of G638 is increased by the C3'-endo pucker of the G620 ribose. This group would actually reside in a closer distance, if the ribose were in a C2'-endo conformation. The offset of the O2' leaves the N1- and N2-groups of G638 free to form hydrogen bonds with the O1P and O2P atoms of A621. The O2P- and O5'-groups of A621 are also in contact with the N1- and N2-groups from G756. All these contacts are consistent with the notion that the A756G mutation affects the transfer of the proton stabilizing the leaving group through a set of contacts that locks the phosphate group, greatly increasing the required activation energy.

The catalytic mechanism of the HdV ribozyme was also investigated following a mutational approach. After publication of the initial crystal structure of the product form of the ribozyme, a construct corresponding to a precursor form of the HdV ribozyme bearing a C75 to U mutation and two additional nucleotides at the 5'-end was studied. Ten crystal structures of this construct were solved in the presence of various divalent cations including magnesium, calcium, strontium, barium, manganese, cobalt, copper and iridium in order to identify both the two players of the acid/base reaction [77]. The C75 to U mutation prevents the de-protonation of the N3 position, thus inactivating the ribozyme. The crystal structures show the presence of an ion in the vicinity of the nucleophile. The model, which could be derived from these complementary studies, is that the cation acts as the general base, abstracting the proton from the 2'-hydroxyl nucleophile U-1, and C75 acts as the general acid, stabilizing the 5'-oxyanion of G1. Another crystal structure containing three consecutive deoxy-residues at the 5'-end of the substrate strand was also published [78]. The original crystal structures of the product form [16] and of the C75U mutated construct [77] were

subject to refinement using the ERRASER program suite in order to rule out structural ambiguities that led to a better interpretation of the catalytic mechanism [79].

6.2.7 Recently discovered ribozymes

In 2015, a set of new ribozymes was identified by comparative genomics analysis [10, 11]. These ribozymes were named after the features of their secondary structures.

Twister is "twisted" by a double pseudoknot, like Twister-sister. Pistol and Hatchett look alike these objects. These ribozymes constitute additional families of endonucleolytic ribozymes, which also yield 5'-hydroxyl and 2',3'-cyclic phosphodiester ends. With the benefit of the acquired knowledge on the crystallization of ribozymes, it took only few years to get crystal structures for most of them. This paragraph is dedicated to those ribozymes and to the strategies that were used to crystallize them.

6.2.7.1 The Twister ribozyme

The Twister ribozyme [10] is widespread within bacteria, fungi, plants and animals. It seems to be important in genetic control, although such a function has not been demonstrated yet. The ~50 nt minimal Twister ribozyme secondary structure is composed of three helices of about four base pairs separated by two internal loops. The crystal structure of the *Oryza sativa* Twister ribozyme illustrates how the ribozyme folds [80]. Basically, the second internal loop adopts a sharp kink allowing stems 2 and 3 to end up side-by-side in a parallel orientation stabilized by the formation of a first pseudoknot (T1) between the apical loop and the 3'-strand of the first internal loop (L1). This conformation is further stabilized by a second pseudoknot (T2) resulting from the

interaction of the 3'-nucleotides from the apical loop with the 5'-strand of the second internal loop (L2). The 5'-strand of the first internal loop contains a UA step where the cleavage occurs. T1 is instrumental in positioning the scissile adenosine residue (Figure 9a, b).

In the construct crystallized by the group of David Lilley [80], catalysis was prevented by the incorporation of a 2'-deoxyuridine (dU) in an RNA entirely chemically synthesized. A crystal packing contact involving the dU perturbs its orientation and is invoked to prevent the observation of the S_N2 -characteristic O2'-P-O5' in-line orientation. The likeliness of an acido-basic based catalytic mechanism was demonstrated by a combination of molecular modeling studies and pH-dependent catalytic measurements of mutated ribozymes. These studies point to an acido-basic cleavage mechanism, like most nucleolytic ribozymes, with G45 as a general base, since a G45 to A mutation shifts the pKa of the reaction. The position of A29 in the crystal structure could not explain thoroughly the acid pKa observed in catalytic measurement experiments, leaving open the question of its involvement. Two other crystal structures of Twister ribozymes from *O. sativa* and from an environmental sample without identification of the organism of origin (*env*) were solved but at lower resolutions and with geometries not permitting to decipher the catalytic mechanism [81].

An additional crystal structure from the group of Patel describing the structure of another environmental Twister ribozyme (*env22*) displays a conformation where a modeled O2' could be properly aligned with the -P-O5' scissile bond [82]. This construct was formed by hybridization of two RNA fragments of 19 and 37 nucleotides obtained by chemical synthesis. The 19-mer contained a dU residue at position 5 to prevent phosphotransfer at residue 6. In this structure, dU5 does not contribute to packing, which rationalizes its better orientation. The structure also confirms the involvement of

G48 (equivalent to *O. sativa* G45) in the acid/base reaction through interaction of its N1-group with a non-bridging oxygen atom of the scissile phosphate. The structure also presents a hexa-coordinated magnesium ion, that seems to be involved in catalysis. Following up, the structure of a mini-Twister ribozyme derived from the *env22* construct was solved, in which stem P1 was depleted, since in-solution studies indicated that it was dispensable for activity [83]. This construct was inactivated by 2'-*O*-methylation of U5. The conformation of the scissile dinucleotide is very close to the one observed in the structure containing a dC5 [82], although the atoms involved in the S_N2 -like mechanism are more off-line than in the dU5 substituted ribozyme, a situation apparently due to the bulkiness of the methyl group that influences the pucker of the ribose ring. Nevertheless, in-depth biochemical studies demonstrated the catalytic role of the magnesium ion coordinating the scissile phosphate as well as of A6. Even-though more studies are necessary to precisely identify the role of each actor, the situation is now that Twister seems to adopt a mixed strategy based on metal ion catalysis on the one hand, and on nucleotide-driven acid/base catalysis on the other hand [83].

6.2.7.2 The twister sister ribozyme

The Twister Sister (TS) ribozyme [11] was named after secondary structure features that look alike those of the Twister ribozyme. However, its 3D structure [84] departs significantly from Twister's, notably by a cleavage site on the 3'-side of the first helix, which forms a distinctive catalytic pocket based on a metal ion with a putative role as a general base activating the nucleophile during catalysis. The 3D structure of the TS ribozyme is organized around two helical stacks weaving tertiary interactions resulting

from the 180° rotation of one helical segment with respect to the other, leading to contacts between the apical loop (L4) and the first internal loop (L1). This twist forms a 3-way junction locked by docking of a couple of unpaired nucleotides in specific receptors through stacking interactions and hydrogen bonding (Figure 9c, d). Like in Twister, L4 is responsible for interactions with the two internal loops, L1 and L2. It provides a receptor for A8, which donates its sugar edge to the sugar edges of G23 and gets stacked in between A25 and A26. G27, the ultimate nucleotide of the apical loop is stretched by the backbone rotamers to reach the most distal region to base pair with C14, providing helical continuity between P2 and A15 from the 3-way junction. In L1, C54 and A55, which comprise the scissile bond, adopt a quasi-helical conformation and appear somehow disconnected from the ribozyme core, except by interaction with a magnesium ion having the O2-atom of C54 in its first shell of hydration. The helical conformation of the nucleotides at the scissile bond is not compatible with the S_N2 -like mechanism and indicates that the structure [84] corresponds to a pre-catalytic state. The RNA strand design strategy was based like in the case of Twister on the depletion of the nucleophilic 2'-hydroxyl group by chemical synthesis of two distinct strands. A ribozyme 40-mer incorporated two 5-bromocytidines, in order to solve the phase problem by anomalous diffraction methods, and a substrate 22-mer incorporated the 2'-deoxycytidine.

In another structure of a TS ribozyme solved by the group of Patel [85], the architecture is based on a 4-way junction and not on a 3-way junction like in the above example. The structure was solved by heavy atom anomalous diffraction methods using iridium hexammine. The 4-way junction as well as an extended L1 internal loop forms a significantly different organization of the overall structure and around the catalytic site. Firstly, the additional stem P3 extends the helical stack formed by P1 and P2 generating

a 4-way junction where the angle between the two helical stacks (P1-P2-P3 and P4-P5) is close to 90°. The expanded L1 provides opportunity for a set of non-canonical base pairs, which also chelate several magnesium ions, in close vicinity of the catalytic site. In spite of a similar strategy was applied to deplete the nucleophile by chemical synthesis of a ribozyme and of a substrate strand incorporating the required modification, the two nucleotides around the scissile bond do not adopt a helical conformation. While L4 serves as a receptor for residue A7 (equivalent to A8 from 5t5a), G35 (equivalent to G27 from 5t5a) interacts with a magnesium ion, which itself is connected to the backbone of the 5'-strand of L1. The intricate set of interactions between L1 and L4 residues seems to promote specific contacts within the purine-rich L1 that lead to the extrusion of the 2'-deoxycytidine residue (C62) in a conformation that could favor the S_N2 -like reaction, since A63 is clamped within the helix by means of hydrogen bonds and stacking interactions locked by magnesium ions. Surprisingly, no ion is observed bridging the A residues from L4 with the groove of L1 as observed in the structure from the group of Lilley [84].

In spite of the application of the same strategy to inactivate the nucleophile by depletion of the 2'-hydroxyl group, these two structures present very different features. The interpretation of the catalytic mechanism needs to be reinforced in one case (5t5a) with specific biochemical studies, whereas in the other case (5y85) the interpretation is more straightforward directly from the structure. The sequences of the ribozymes themselves seem to be responsible for these observations and point to the difficulty to yield exploitable structural data to shed light on catalytic mechanisms.

6.2.7.3 The Pistol ribozyme

Crystal structures of the Pistol ribozyme were solved quickly after its discovery and the first functional studies [86, 87]. The *env25* ribozyme [86] was made up of two chemically synthesized annealed strands, an 11-mer substrate strand, and a 47-mer ribozyme core. The *env27* ribozyme was made up of a 15 nt substrate, while the core was obtained by in vitro transcription [87]. In both cases, cleavage was prevented by incorporation of a deoxy residue in place of G53 (*env25*) or G10 (*env27*). The secondary structure is composed of a short hairpin followed by a longer one. The latter is interrupted by a very asymmetric internal loop, the longest strand of which forms a half-helical turn pseudoknot with the loop of the former hairpin. In the 3D structure, the pseudoknot is clamped between stems P1 and P3, making an extended helical core. The strand connecting P1 to P2 elegantly follows the shallow groove of P1 and sets P2 off the ribozyme core. Since the final structures showed very similar features, we describe details from the *env25* structure. This arrangement, together with the constraints due to the formation of the P2 helix, produces the sharp kink necessary to splay apart the nucleotides around the scissile phosphate group of C54 (Figure 6.2.10).

Initial biochemical analysis [88], NMR and fluorescence spectroscopy data obtained on the crystallized forms of the ribozymes point to the N3 group of A32 to be responsible for stabilization of the 5'-oxyanion leaving group, while G40 would be able to activate the nucleophile. The dG modification does not prevent to observe a magnesium ion close to the scissile phosphate. However, this ion seems to play a structural role rather than a catalytic one, since it is not directly coordinated to any RNA atom.

6.2.8 Conclusions and perspectives

All the examples reported in this review show how structural models offer a powerful heuristic framework to design and interpret the results of biochemical and mutational studies toward a better understanding of the catalytic mechanisms of ribozymes. This means that even-though significant knowledge is required to inactivate the ribozyme to crystallize, it is from the structures obtained that the conclusive experiments may be designed. Efficient and diverse strategies for controlling ribozyme catalysis in the context of crystallization studies is thus a valuable addition to the biochemist's toolbox. In these strategies, the solid phase chemical synthesis of oligonucleotides holds a central role.

Technical progresses in chemical and enzymatic synthesis, in heavy atom derivatization of RNA, in softwares both for RNA folding predictions and crystal structure refinement as well as data collection and treatment, and in detector sensitivity allow for solving RNA structures always faster. The main bottleneck remains crystallization, since the stability of an RNA molecule does not only depend on its architecture, but also on its folding process, as well as on the crystal packing. In the future, x-ray free electron laser (XFEL) facilities may help to release the pressure on obtaining large crystals, as in a recent study, in which distinct forms of a riboswitch could be observed simultaneously, [89] and thus become a more routine technic.

To summarize, the modifications, which require lesser knowledge on catalysis are the deoxy substitution of the nucleophile or its methylation. Another strategy consists in using a split substrate and results in the loss of the scissile phosphate. All these modifications perturb the catalytic site organization, and structural interpretations should be made with the support of biochemical data obtained on the unmodified ribozyme form. The construction of a circularly permuted ribozyme is always possible

and mimics the split substrate strategy. In this case, in vitro transcription can be used to produce a single strand RNA of any length opening up the possibility to purify the RNA of interest under native conditions directly from the transcription mix. Finally, studying the transition state structural mimic using a vanadate ion constitutes a fourth strategy that can be added on top of the split substrate or circular permutation. When nucleotide candidates involved in nucleophile activation or leaving group stabilization are identified, it is also possible to design mutated constructs with very poor catalytic properties.

6.2.9 Acknowledgement

BM is supported by CNRS and by the LabEx MitoCross (LABEX ANR-11-LABX-0057_MITOCROSS). DS is supported by an IdEx doctoral grant obtained from the University of Strasbourg (BGPC 17/N° ARC 26349). MC acknowledges funding from BIG LidEx program.

6.2.10 References

1. Guerrier-Takada, C., Gardiner, K., Marsh, T., Pace, N., and Altman, S. (1983) The RNA moiety of ribonuclease P is the catalytic subunit of the enzyme. *Cell* **35**, 849-857.
2. Cech, T. R. (2000) The Ribosome Is a Ribozyme. *Science* **289** (5481), 878-879 %R 810.1126/science.1289.5481.1878.
3. Galej, W. P., Toor, N., Newman, A. J., and Nagai, K. (2018) Molecular Mechanism and Evolution of Nuclear Pre-mRNA and Group II Intron Splicing: Insights from Cryo-Electron Microscopy Structures. *Chem Rev.*
4. Hutchins, C. J., Rathjen, P. D., Forster, A. C., and Symons, R. H. (1986) Self-cleavage of plus and minus RNA transcripts of avocado sunblotch viroid. *Nucleic Acids Res.* **14** (9), 3629-3640.
5. Buzayan, J. M., Gerlach, W. L., and Bruening, G. (1986) Non-enzymatic cleavage and ligation of RNAs complementary to a plant virus satellite RNA. *Nature* **323**, 349-353.
6. Sharmeen, L., Kuo, M. Y.-P., Dinter-Gottlieb, G., and Taylor, J. (1988) Antigenomic RNA of human hepatitis delta virus can undergo self-cleavage. *J. Virol.* **62**, 2674-2679.
7. Saville, B. J. and Collins, R. A. (1990) A site-specific self-cleavage reaction performed by a novel RNA in *Neurospora* mitochondria. *Cell* **61**, 685-696.
8. Cech, T. R., Zaug, A. J., and Grabowski, P. J. (1981) In vitro splicing of the ribosomal RNA precursor of *Tetrahymena*: Involvement of a guanosine nucleotide in the excision of the intervening sequence. *Cell* **27**, 487-496.
9. Michel, F., Jaquier, A., and Dujon, B. (1982) Comparison of fungal mitochondrial introns reveals extensive homologies in RNA secondary structure. *Biochimie* **64**, 867-881.
10. Roth, A., *et al.* (2014) A widespread self-cleaving ribozyme class is revealed by bioinformatics. *Nat Chem Biol* **10** (1), 56-60.
11. Weinberg, Z., *et al.* (2015) New classes of self-cleaving ribozymes revealed by comparative genomics analysis. *Nat Chem Biol* **11** (8), 606-610.
12. Winkler, W. C., Nahvi, A., Roth, A., Collins, J. A., and Breaker, R. R. (2004) Control of gene expression by a natural metabolite-responsive ribozyme. *Nature* **428** (6980), 281-286.
13. Kondo, J., Sauter, C., and Masquida, B. [2014] RNA crystallization, in *Handbook of RNA biochemistry*, [eds Hartmann, R. K., Bindereif, A., Schön, A., and Westhof, E.], Wiley VCH Verlag GmbH & Co, pp 481-498.
14. Lilley, D. M. J. (2017) How RNA acts as a nuclease: some mechanistic comparisons in the nucleolytic ribozymes. *Biochemical Society transactions* **45** (3), 683-691.
15. Raines, R. T. (1998) Ribonuclease A. *Chem Rev* **98** (3), 1045-1066.
16. Ferré-D'Amaré, A. R., Zhou, K. H., and Doudna, J. A. (1998) Crystal structure of a hepatitis delta virus ribozyme. *Nature* **395** (6702), 567-574.
17. Klein, D. J. and Ferré-D'Amare, A. R. (2006) Structural basis of glmS ribozyme activation by glucosamine-6-phosphate. *Science* **313** (5794), 1752-1756.
18. Cochrane, J. C., Lipchock, S. V., and Strobel, S. A. (2007) Structural investigation of the GlmS ribozyme bound to its catalytic cofactor. *Chemistry & biology* **14** (1), 97-105.

19. Ferre-D'Amare, A. R. and Doudna, J. A. (2000) Crystallization and structure determination of a hepatitis delta virus ribozyme: use of the RNA-binding protein U1A as a crystallization module. *Journal of molecular biology* **295** (3), 541-556.
20. Sussman, J. L., Holbrook, S. R., Warrant, R. W., Church, G. M., and Kim, S.-H. (1978) Crystal structure of yeast phenylalanine tRNA. I. Crystallographic refinement. *J. Mol. Biol.* **123**, 607-630.
21. Westhof, E., Dumas, P., and Moras, D. (1985) Crystallographic refinement of yeast aspartic acid transfer RNA. *Journal of molecular biology* **184**, 119-145.
22. Pley, H. W., Flaherty, K. M., and McKay, D. B. (1994) Three-dimensional structure of a hammerhead ribozyme. *Nature*. **372** (3 Nov), 68-74.
23. Scott, W. G., Finch, J. T., and Klug, A. (1995) The crystal structure of an all-RNA hammerhead ribozyme : A proposed mechanism for RNA catalytic cleavage. *Cell*. **81**, 991-1002.
24. Cate, J. H., *et al.* (1996) Crystal structure of a group I ribozyme domain: principles of RNA packing. *Science*. **273**, 1678-1684.
25. Branch, A. D. and Robertson, H. D. (1984) A replication cycle for viroids and other small infectious RNA's. *Science* **223** (4635), 450-455.
26. Tanner, M. A., Anderson, E. M., Gutell, R. R., and Cech, T. R. (1997) Mutagenesis and comparative sequence analysis of a base triple joining the two domains of group I ribozymes. *Rna* **3** (9), 1037-1051.
27. Shih, I. H. and Been, M. D. (2001) Involvement of a cytosine side chain in proton transfer in the rate-determining step of ribozyme self-cleavage. *Proceedings of the National Academy of Sciences of the United States of America* **98** (4), 1489-1494.
28. Nakano, S., Proctor, D. J., and Bevilacqua, P. C. (2001) Mechanistic characterization of the HDV genomic ribozyme: assessing the catalytic and structural contributions of divalent metal ions within a multichannel reaction mechanism. *Biochemistry* **40** (40), 12022-12038.
29. Luptak, A., Ferre-D'Amare, A. R., Zhou, K., Zilm, K. W., and Doudna, J. A. (2001) Direct pK(a) measurement of the active-site cytosine in a genomic hepatitis delta virus ribozyme. *Journal of the American Chemical Society* **123** (35), 8447-8452.
30. Milewski, S. (2002) Glucosamine-6-phosphate synthase--the multi-facets enzyme. *Biochimica et biophysica acta* **1597** (2), 173-192.
31. Savinov, A. and Block, S. M. (2018) Self-cleavage of the glmS ribozyme core is controlled by a fragile folding element. *Proceedings of the National Academy of Sciences of the United States of America*.
32. Klein, D. J. and Ferre-D'Amare, A. R. (2009) Crystallization of the glmS ribozyme-riboswitch. *Methods in molecular biology* **540**, 129-139.
33. Jimenez, R. M., Delwart, E., and Luptak, A. (2011) Structure-based search reveals hammerhead ribozymes in the human microbiome. *The Journal of biological chemistry* **286** (10), 7737-7743.
34. Fedor, M. J. and Uhlenbeck, O. C. (1990) Substrate sequence effects on "hammerhead" RNA catalytic efficiency. *Proceedings of the National Academy of Sciences of the United States of America* **87** (5), 1668-1672.
35. Ruffner, D. E., Dahm, S. C., and Uhlenbeck, O. C. (1989) Studies on the hammerhead RNA self-cleaving domain. *Gene* **82** (1), 31-41.
36. Caruthers, M. H. (2011) A brief review of DNA and RNA chemical synthesis. *Biochemical Society transactions* **39** (2), 575-580.

37. Hartsel, S. A., Kitchen, D. E., Scaringe, S. A., and Marshall, W. S. (2005) RNA oligonucleotide synthesis via 5'-silyl-2'-orthoester chemistry. *Methods in molecular biology* **288**, 33-50.
38. Scott, W. G., Murray, J. B., Arnold, J. R. P., Stoddard, B. L., and Klug, A. (1996) Capturing the structure of a catalytic RNA intermediate: The hammerhead ribozyme. *Science*. **274**, 2065-2069.
39. Khvorova, A., Lescoute, A., Westhof, E., and Jayasena, S. D. (2003) Sequence elements outside the hammerhead ribozyme catalytic core enable intracellular activity. *Nature structural biology* **10** (9), 708-712.
40. Canny, M. D., *et al.* (2004) Fast cleavage kinetics of a natural hammerhead ribozyme. *Journal of the American Chemical Society* **126** (35), 10848-10849.
41. Martick, M. and Scott, W. G. (2006) Tertiary contacts distant from the active site prime a ribozyme for catalysis. *Cell* **126** (2), 309-320.
42. Nelson, J. A. and Uhlenbeck, O. C. (2006) When to believe what you see. *Molecular cell* **23** (4), 447-450.
43. Adams, P. L., Stahley, M. R., Kosek, A. B., Wang, J., and Strobel, S. A. (2004) Crystal structure of a self-splicing group I intron with both exons. *Nature* **430** (6995), 45-50.
44. Adams, P. L., *et al.* (2004) Crystal structure of a group I intron splicing intermediate. *Rna* **10** (12), 1867-1887.
45. Ferre-D'Amare, A. R. (2010) Use of the spliceosomal protein U1A to facilitate crystallization and structure determination of complex RNAs. *Methods*.
46. Stahley, M. R. and Strobel, S. A. (2005) Structural evidence for a two-metal-ion mechanism of group I intron splicing. *Science* **309** (5740), 1587-1590.
47. Guo, F., Gooding, A. R., and Cech, T. R. (2004) Structure of the tetrahymena ribozyme; base triple sandwich and metal ion at the active site. *Molecular cell* **16** (3), 351-362.
48. Golden, B. L., Kim, H., and Chase, E. (2005) Crystal structure of a phage Twort group I ribozyme-product complex. *Nature structural & molecular biology* **12** (1), 82-89.
49. Lambowitz, A. M. and Belfort, M. (2015) Mobile Bacterial Group II Introns at the Crux of Eukaryotic Evolution. *Microbiol Spectr* **3** (1), MDNA3-0050-2014.
50. Costa, M., Walbott, H., Monachello, D., Westhof, E., and Michel, F. (2016) Crystal structures of a group II intron lariat primed for reverse splicing. *Science* **354** (6316).
51. Hampel, A., Tritz, R., Hicks, M., and Cruz, P. (1990) 'Hairpin' catalytic RNA model : evidence for helices and sequence requirement for substrate RNA. *Nuc. Ac. Res.* **18** (2), 299-304.
52. Murchie, A. I. H., Thomson, J. B., Walter, F., and Lilley, D. M. (1998) Folding of the hairpin in its natural conformation achieves close physical proximity of the loops. *Mol. Cell.* **1** (6), 873-881.
53. Walter, N. G., Burke, J. M., and Millar, D. P. (1999) Stability of hairpin ribozyme tertiary structure is governed by the interdomain junction. *Nature structural biology* **6** (6), 544-549.
54. McKinney, S. A., *et al.* (2004) Single-molecule studies of DNA and RNA four-way junctions. *Biochemical Society transactions* **32** (Pt 1), 41-45.
55. Lilley, D. M. and Norman, D. G. (1999) The Holliday junction is finally seen with crystal clarity. *Nature structural biology* **6** (10), 897-899.

56. Rupert, P. B. and Ferre-D'Amare, A. R. (2001) Crystal structure of a hairpin ribozyme-inhibitor complex with implications for catalysis. *Nature* **410** (6830), 780-786.
57. Rupert, P. B., Massey, A. P., Sigurdsson, S. T., and Ferre-D'Amare, A. R. (2002) Transition state stabilization by a catalytic RNA. *Science* **298** (5597), 1421-1424.
58. Mir, A., *et al.* (2015) Two Divalent Metal Ions and Conformational Changes Play Roles in the Hammerhead Ribozyme Cleavage Reaction. *Biochemistry* **54** (41), 6369-6381.
59. Mir, A. and Golden, B. L. (2016) Two Active Site Divalent Ions in the Crystal Structure of the Hammerhead Ribozyme Bound to a Transition State Analogue. *Biochemistry* **55** (4), 633-636.
60. Meyer, M., *et al.* (2014) Speciation of a group I intron into a lariat capping ribozyme. *Proceedings of the National Academy of Sciences of the United States of America* **111** (21), 7659-7664.
61. Nielsen, H., Westhof, E., and Johansen, S. (2005) An mRNA is capped by a 2', 5' lariat catalyzed by a group I-like ribozyme. *Science* **309** (5740), 1584-1587.
62. Tang, Y., Nielsen, H., Masquida, B., Gardner, P. P., and Johansen, S. D. (2014) Molecular characterization of a new member of the lariat capping twin-ribozyme introns. *Mob DNA* **5**, 25.
63. Meyer, M. and Masquida, B. (2014) Cis-Acting 5' Hammerhead Ribozyme Optimization for In Vitro Transcription of Highly Structured RNAs. *Methods in molecular biology* **1086**, 21-40.
64. Li, X., Yang, L., and Chen, L. L. (2018) The Biogenesis, Functions, and Challenges of Circular RNAs. *Molecular cell* **71** (3), 428-442.
65. Franz, A., *et al.* (2018) Circular RNAs: a new class of biomarkers as a rising interest in laboratory medicine. *Clin Chem Lab Med.*
66. Plagens, A., Daume, M., Wiegel, J., and Randau, L. (2015) Circularization restores signal recognition particle RNA functionality in *Thermoproteus*. *eLife* **4**.
67. Hammann, C., Luptak, A., Perreault, J., and de la Pena, M. (2012) The ubiquitous hammerhead ribozyme. *Rna* **18** (5), 871-885.
68. Webb, C. H. and Luptak, A. (2011) HDV-like self-cleaving ribozymes. *RNA biology* **8** (5).
69. Gott, J. M., Pan, T., LeCuyer, K. A., and Uhlenbeck, O. C. (1993) Using circular permutation analysis to redefine the R17 coat protein binding site. *Biochemistry* **32** (49), 13399-13404.
70. Harris, M. E. and Christian, E. L. (1999) Use of circular permutation and end modification to position photoaffinity probes for analysis of RNA structure. *Methods* **18** (1), 51-59.
71. Ohuchi, S. J., Sagawa, F., Sakamoto, T., and Inoue, T. (2015) Altering the orientation of a fused protein to the RNA-binding ribosomal protein L7Ae and its derivatives through circular permutation. *Biochem Biophys Res Commun* **466** (3), 388-392.
72. Truong, J., Hsieh, Y. F., Truong, L., Jia, G., and Hammond, M. C. (2018) Designing fluorescent biosensors using circular permutations of riboswitches. *Methods.*
73. Pan, T., Fang, X., and Sosnick, T. (1999) Pathway modulation, circular permutation and rapid RNA folding under kinetic control. *Journal of molecular biology* **286** (3), 721-731.
74. Suslov, N. B., *et al.* (2015) Crystal structure of the Varkud satellite ribozyme. *Nat Chem Biol* **11** (11), 840-846.

75. Fernandez-Millan, P., *et al.* (2016) Transfer RNA: From pioneering crystallographic studies to contemporary tRNA biology. *Arch Biochem Biophys* **602**, 95-105.
76. Wilson, T. J. and Lilley, D. M. (2011) Do the hairpin and VS ribozymes share a common catalytic mechanism based on general acid-base catalysis? A critical assessment of available experimental data. *Rna* **17** (2), 213-221.
77. Ke, A., Zhou, K., Ding, F., Cate, J. H., and Doudna, J. A. (2004) A conformational switch controls hepatitis delta virus ribozyme catalysis. *Nature* **429** (6988), 201-205.
78. Chen, J. H., *et al.* (2010) A 1.9 Å crystal structure of the HDV ribozyme precleavage suggests both Lewis acid and general acid mechanisms contribute to phosphodiester cleavage. *Biochemistry* **49** (31), 6508-6518.
79. Kapral, G. J., *et al.* (2014) New tools provide a second look at HDV ribozyme structure, dynamics and cleavage. *Nucleic Acids Res* **42** (20), 12833-12846.
80. Liu, Y., Wilson, T. J., McPhee, S. A., and Lilley, D. M. (2014) Crystal structure and mechanistic investigation of the twister ribozyme. *Nat Chem Biol* **10** (9), 739-744.
81. Eiler, D., Wang, J., and Steitz, T. A. (2014) Structural basis for the fast self-cleavage reaction catalyzed by the twister ribozyme. *Proceedings of the National Academy of Sciences of the United States of America* **111** (36), 13028-13033.
82. Ren, A., *et al.* (2014) In-line alignment and Mg(2)(+) coordination at the cleavage site of the env22 twister ribozyme. *Nature communications* **5**, 5534.
83. Kosutic, M., *et al.* (2015) A Mini-Twister Variant and Impact of Residues/Cations on the Phosphodiester Cleavage of this Ribozyme Class. *Angew Chem Int Ed Engl* **54** (50), 15128-15133.
84. Liu, Y., Wilson, T. J., and Lilley, D. M. J. (2017) The structure of a nucleolytic ribozyme that employs a catalytic metal ion. *Nat Chem Biol* **13** (5), 508-513.
85. Zheng, L., *et al.* (2017) Structure-based insights into self-cleavage by a four-way junctional twister-sister ribozyme. *Nature communications* **8** (1), 1180.
86. Ren, A., *et al.* (2016) Pistol ribozyme adopts a pseudoknot fold facilitating site-specific in-line cleavage. *Nature Chemical Biology* **12**, 702.
87. Nguyen, L. A., Wang, J., and Steitz, T. A. (2017) Crystal structure of Pistol, a class of self-cleaving ribozyme. *Proceedings of the National Academy of Sciences of the United States of America* **114** (5), 1021-1026.
88. Harris, K. A., Lunse, C. E., Li, S., Brewer, K. I., and Breaker, R. R. (2015) Biochemical analysis of pistol self-cleaving ribozymes. *Rna* **21** (11), 1852-1858.
89. Stagno, J. R., *et al.* (2017) Structures of riboswitch RNA reaction states by mix-and-inject XFEL serial crystallography. *Nature* **541** (7636), 242-246.
90. Leontis, N. B. and Westhof, E. (2001) Geometric nomenclature and classification of RNA base pairs. *Rna* **7** (4), 499-512.

Figure legends

Figure 6.2.1: The folded core of the HdV (a) and GlmS (b) ribozymes corresponds to the 3'-cleavage products. Each panel presents the secondary structure of the ribozyme facing the corresponding crystal structure. The arrow indicates the position of the cleavage site upstream from the 5'-end. The structural elements are color-coded identically on the secondary and three-dimensional (3D) structures pictures. The 3D structures have been derived from pdb files 1drs and 3g9c for HdV and GlmS ribozymes, respectively. The substrate strands are depicted in blue and the ribozyme strands in orange. The tertiary interaction between the loop from stem II and the internal loop from stem I is depicted in light blue using the Leontis-Westhof nomenclature [90].

Figure 6.2.2: The GlmS riboswitch is also a ribozyme. (a) The GlmS riboswitch does not change drastically its conformation upon binding of the GlcN6P. Rather, it undergoes cleavage of its 5'-sequence, which leads to degradation of the mRNA (sketched as a dashed line) In bacteria, strand cleavage leads to splitting the Shine-Dalgarno sequence from the start codon. (b) The secondary structure of the *Bacillus anthracis* riboswitch is depicted with the guanosine that has been flagged as an important residue for GlcN6P binding. The region where the latter binds is framed in a grey square. (c) The 3D structure of the riboswitch (PDB: 3g9c) is represented on this panel with the same color code as in (b).

Figure 6.2.3: This figure displays the structures of the minimal (pdb: 1mme) (a) and the extended (pdb: 3zd5) (c) versions of the hammerhead ribozyme. Panels (b) and (d) show how the residues around the scissile bond are organized according to the absence

or presence of the tertiary interaction (b: cyan) between the loop of stem II and the internal loop of stem I, respectively. It is straightforward from (d) that the three atoms involved in the S_N2 -like reaction are ideally aligned, with respect to (b).

Figure 6.2.4: (a) Splicing pathway mediated by the group I introns in general (see text for details). (b) Secondary structure depicting the tertiary interactions observed in the 3D structure (c). The residues that have been modified as deoxynucleotides are framed in grey on the secondary structure diagram and represented in sticks mode on the 3D panel, showing how they are close in space. The U1A protein and the RNA binding site are visible in the lower right corner. These modified nucleotides were integrated in two distinct oligonucleotides. The first one constitutes a short 5'-exon forming P1 (5'-CAU-3'). The second one spans from residue 190 up to the 3'-end of P10. The conformation corresponds to the pre-cleavage state prior to the second catalytic step (see panel a).

Figure 6.2.5: Structure of a group II intron lariat primed for reverse splicing. (a) Secondary structure outline, colored by domains, of the crystallized group II intron lariat. The intron crystallized is an engineered version of the *Oceanobacillus iheyensis* group II ribozyme [50]. Only the active site nucleotides or those involved in binding of the catalytic metal ions are shown. The RNA oligonucleotide corresponding to the unreactive analog of the 5'-exon used for co-crystallization is shown in cyan with the 3'-terminal nucleotide $m^5U3'H$ standing for a 5-methyluridine with a 3'-deoxyribose (the m^5 base modification was imposed by the chemical synthesis of the 7-mer RNA and did not interfere with base-pairing of the oligonucleotide to the intron lariat). The arrow spanning a section of the terminal loop in subdomain ID2 indicates the 5'-exon binding site, which is complementary to the sequence of the 5'-exon. (b) Crystal structure of the

group II intron lariat bound to its 5'-exon RNA at 3.5 Å resolution (PDB entry 5j02). Coloring of the structure is according to panel a. (c) Close-up view of the active site showing the network of hydrogen bonds (dashed black lines) and stacking interactions that involve the 2',5'-branch nucleotides, the intron boundaries and the conserved γ nucleotide. The architecture of the active site directly promotes positioning of the terminal ribose of the lariat into the reaction center in a configuration poised for catalysis of the reverse splicing reaction. The catalytic metal ions (Y1/M1 and Y2) identified in the reaction center establish inner-sphere coordinations (dashed yellow lines) with the 2'- and 3'-hydroxyl groups of the last intron nucleotide (γ') and the non-bridging phosphate oxygens of highly conserved nucleotides of domain V (these nucleotides are numbered in panel a). The asterisk indicates that the terminal ribose of the 5'-exon analog lacks a 3'-hydroxyl group.

Figure 6.2.6: The hairpin ribozyme can be active as a short or an extended version, provided that the internal loops of domains A and B establish specific interactions. In the short version (a), domains A and B are tethered by a flexible linker, whereas in the natural context, a four-way junction is formed (b). The black arrow points to the cleavage site. Panel (c) displays the 3D structure corresponding to panel (b) (pdb: 1m5k). The orange substrate strand bound in trans in the RNA construct extends through domain b and stem c. The topology of the 4-way junction is clearly visible on panel (c). Panel (d) shows a close-up of the scissile di-nucleotide (orange) embedded in the ribozyme core (blue). The curved arrows show how the electrons are supposedly transferred during catalysis from the O2'-hydroxyl group of A9 to the O5' of G10. (e) The vanadate complex (pdb: 1m5o) mimicking the transition state in a similar orientation

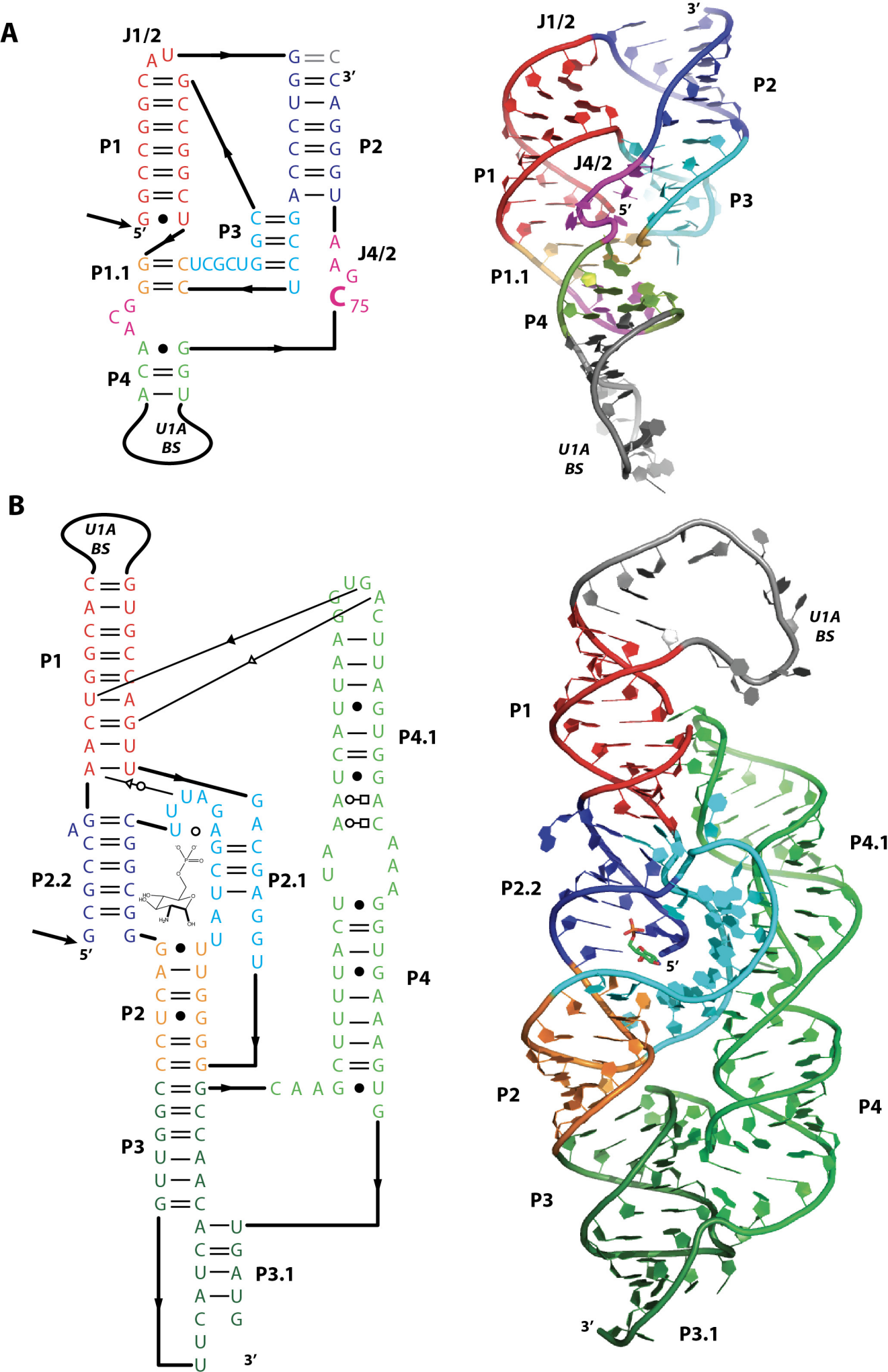
shows that G1 still interacts within loop B with residue C25 (blue sticks). The presence of vanadate perturbs significantly the pucker of the A-1 ribose moiety.

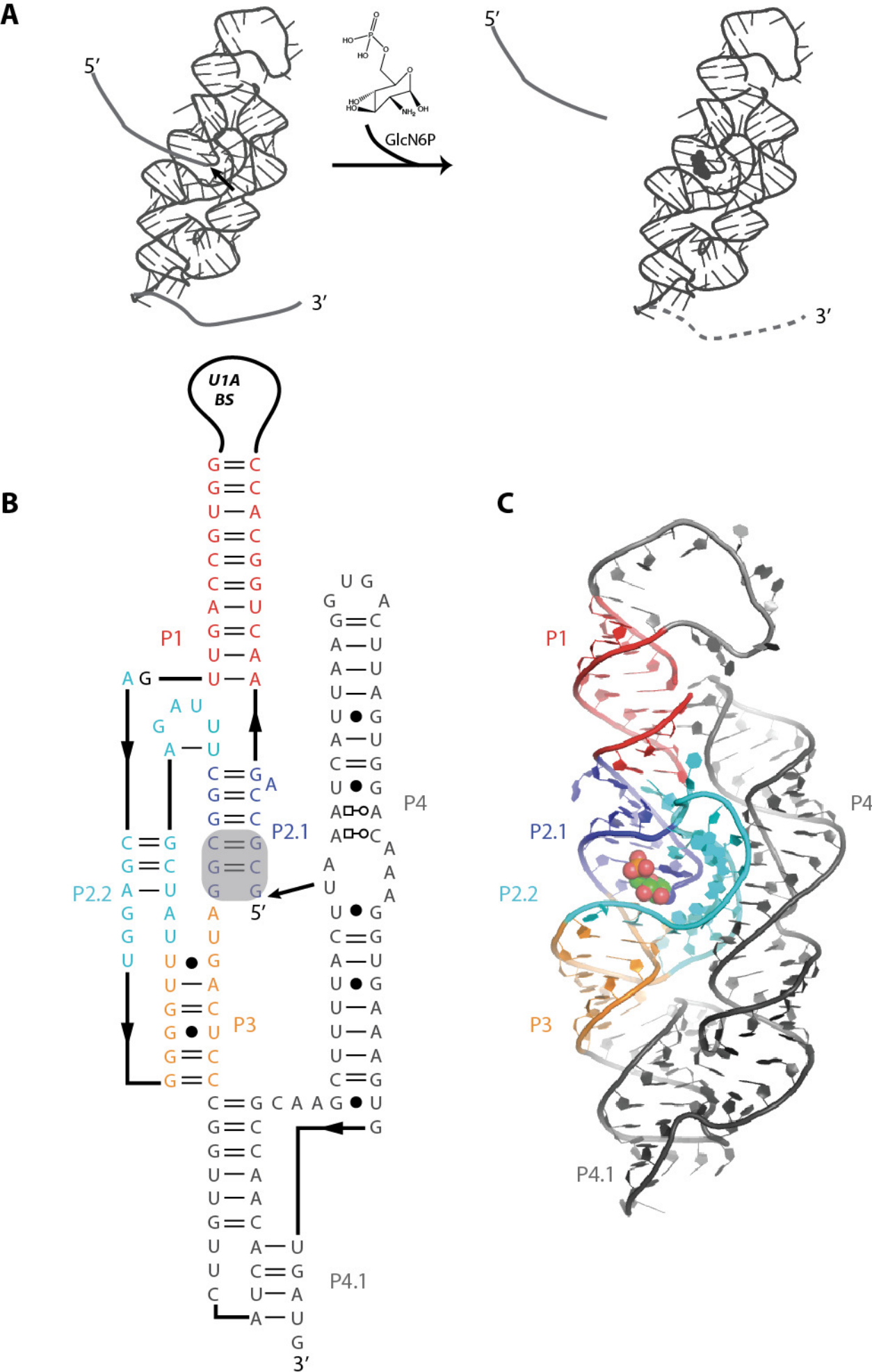
Figure 6.2.7: Organization of the LC ribozyme constructs. (a) Representation of the secondary structure of the wild-type LC ribozyme. Both the 5'- and 3'- ends originate from DP2. The 3'-G residue from the ribozyme (ω G, blue circle), is tethered to the three lariat forming nucleotides (orange circles). In the circularly permuted (CP) construct (b), the 5'- and 3'-ends are placed at the lariat C, and ribozyme ω G, respectively. The continuity of the RNA chain is preserved by closing DP2 using a UUCG loop (green circles). The secondary structure and tertiary interactions deduced from the crystal structure of the CP construct are represented on panel (c).

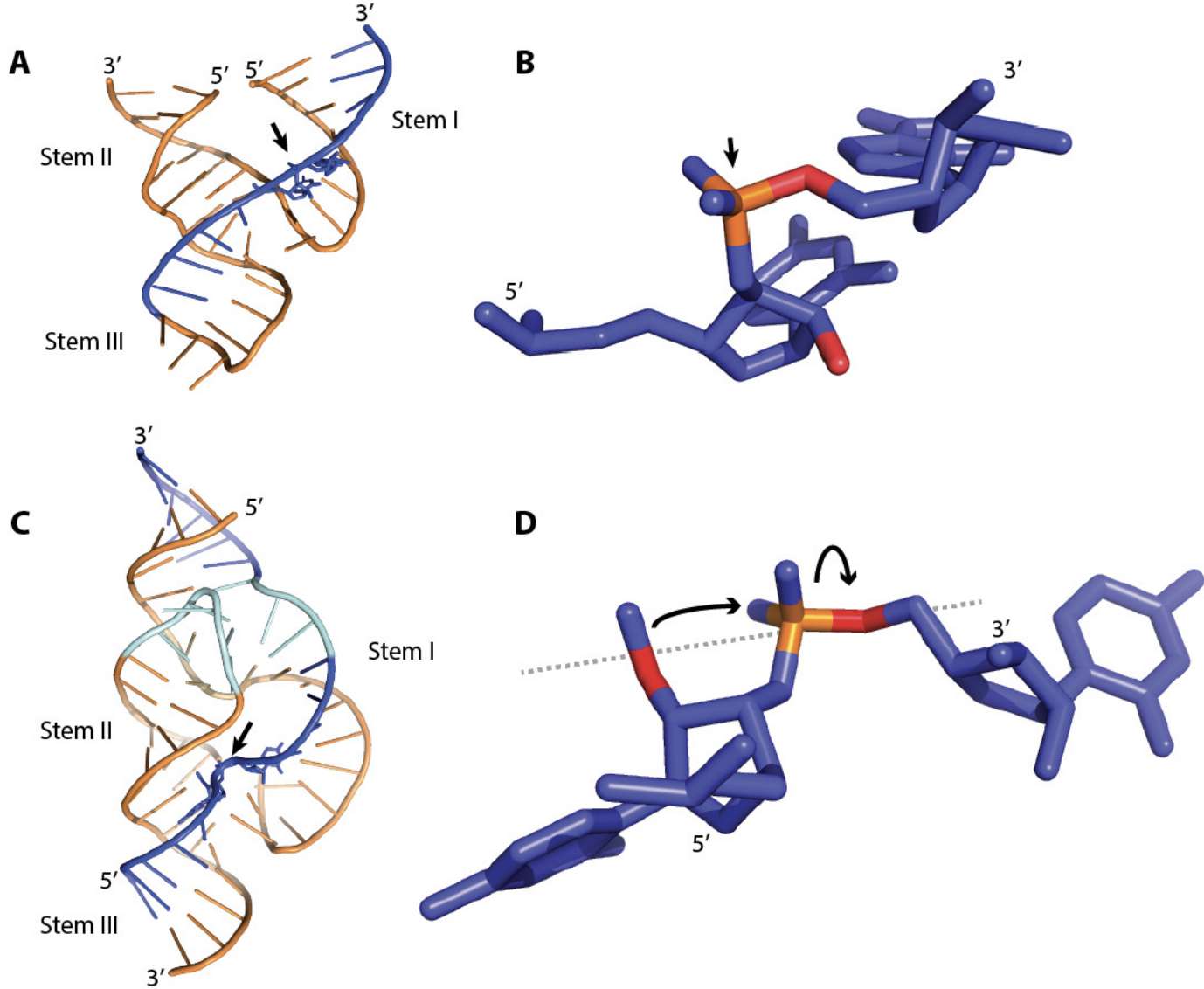
Figure 6.2.8: The secondary structure of the crystallized construct of the VS ribozyme (a) shows how the three 3-way junctions in the VS ribozyme lead to co-axial stacking of helices 1 to 4 (bold face numbers). The residues around the scissile phosphate (G620-A621) and the general base (G638) and acid (A756) are framed in a colored circle (orange for the RNA containing the scissile phosphate, and grey for the RNA interacting in trans). (b) 3D structure of the VS ribozyme dimer. The molecule corresponding to panel (a) is represented using the same color code. The ribozyme interacting in trans is grey colored. (c) The close-up of the catalytic site in the G638A mutant crystal structure (pdb 4r4v) shows how the residues around the scissile phosphate of A621 are splayed apart, and the cross-strand stacking between residues 638 and 620. (d) These features are maintained in the A756G mutant crystal structure (pdb 4r4p). However, the presence of two G residues weaves a set of hydrogen bonds to the scissile phosphate that is not observed for the G638A mutant.

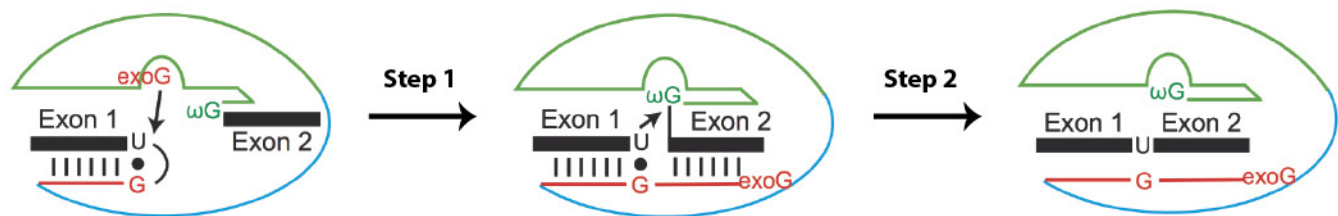
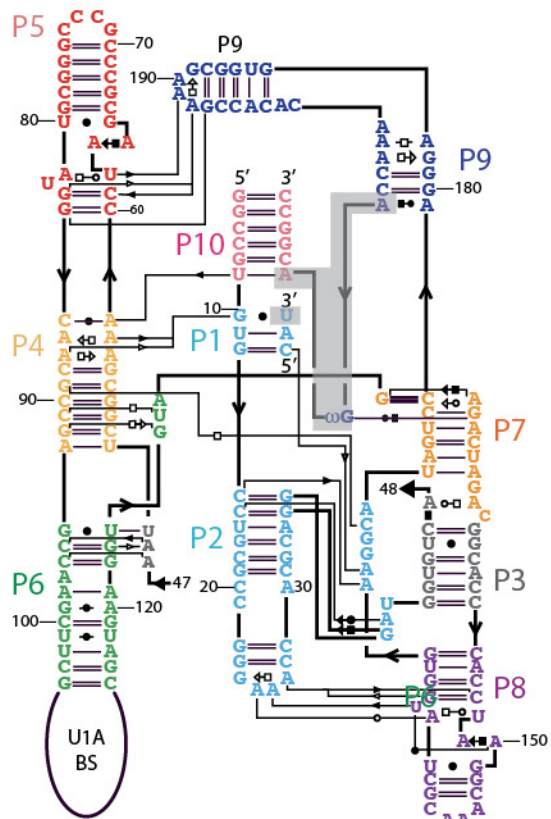
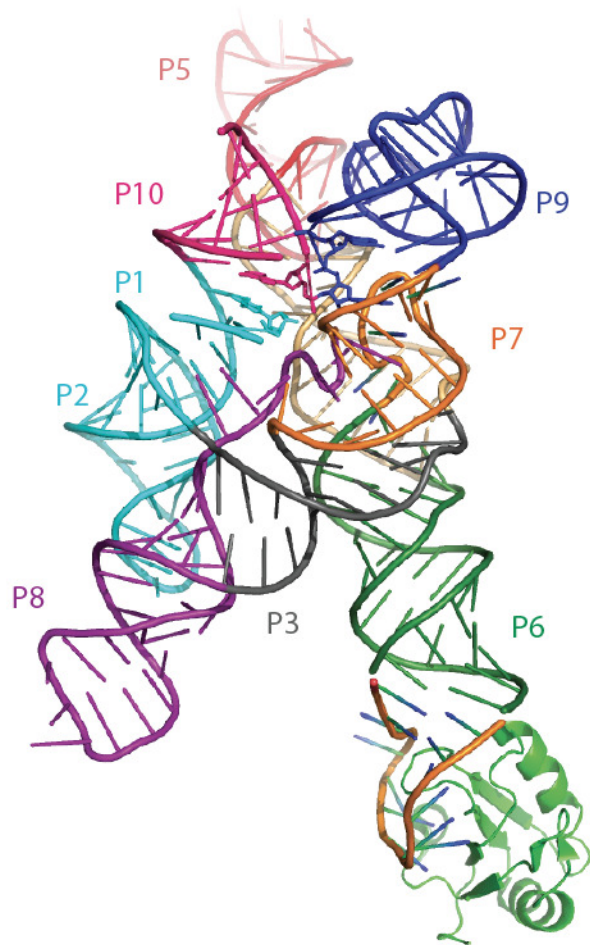
Figure 6.2.9: The Twister (a, b) and Twister Sister (TS) (c, d) ribozymes. In spite of similarities at the secondary structure level, these two ribozymes adopt distinct architectures as can be seen from the secondary structures deduced from the 3D structures. The cleavage sites are indicated by short black arrows on all panels. The structure of the Twister ribozyme from *Oryza sativa* is represented (a, b) from pdb file 4oji. The structure of the Twister Sister ribozyme prepared from pdb file 5t5a is represented on panels c and d.

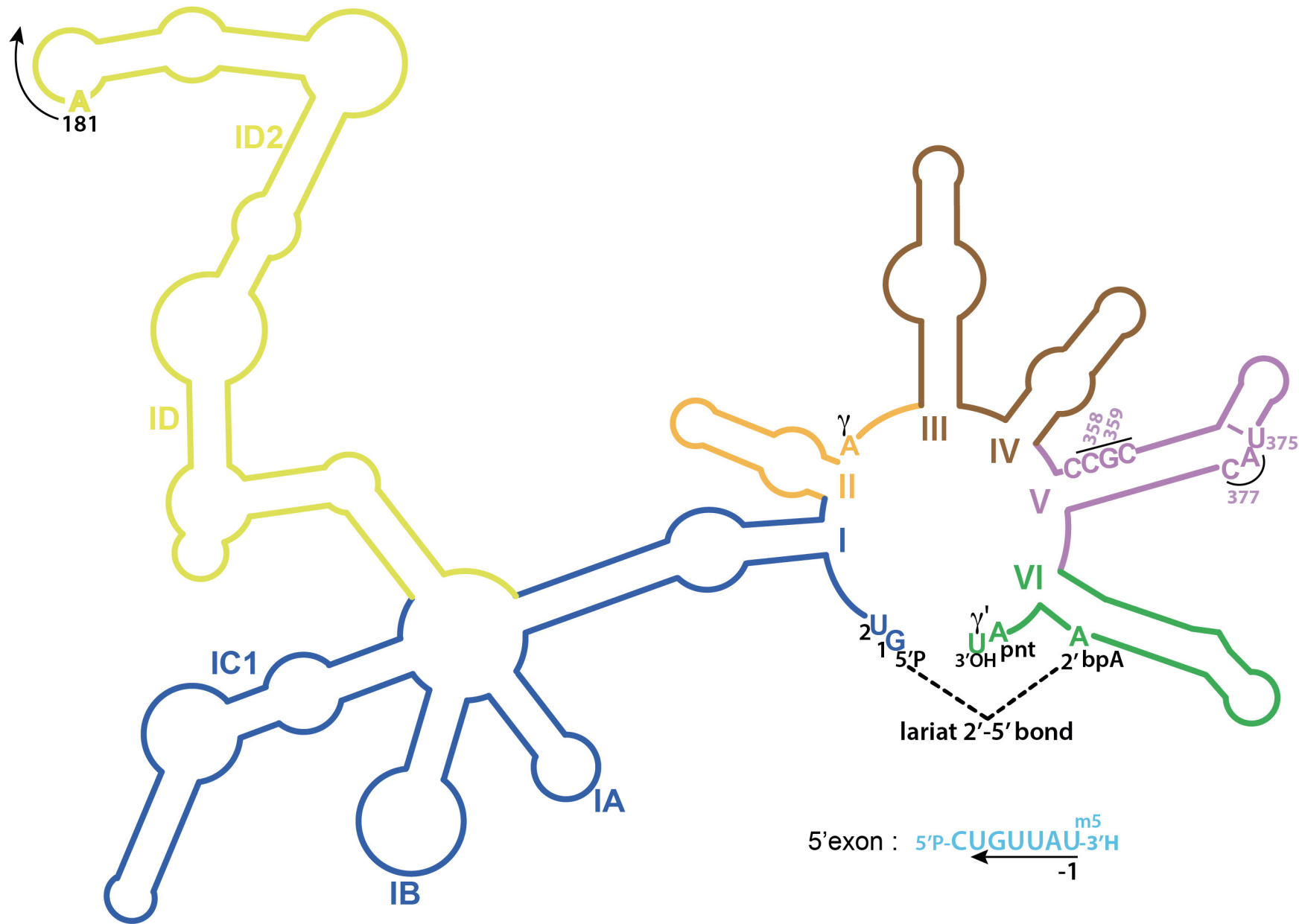
Figure 6.2.10: Structural aspects of the Pistol ribozyme (pdb 5k7e). (a) The secondary structure shows the topology of the RNA, emphasizing how Pk is made from the interactions of the two loops. (b) The overall 3D structure shows how P1, Pk and P2 stack on each other to form an extended helical core on the side, of which P2 docks and induces the kink at the cleavage site. (c) A close-up of the catalytic site shows the kink at the scissile phosphate between G53 and U54. Distances between atomic groups that could be important during the catalytic reaction are indicated by yellow dashed lines (G40(N1)-U54(O1P) 4.0 Å; G40(N2)-U54(O1P) 4.1 Å; G40(N1)-G53(C2') 3.5 Å; Mg-U54(P) 4.1 Å; A32(O2')-U54(O5') 5.1 Å; A32(N3)-U54(O5') 5.4 Å).

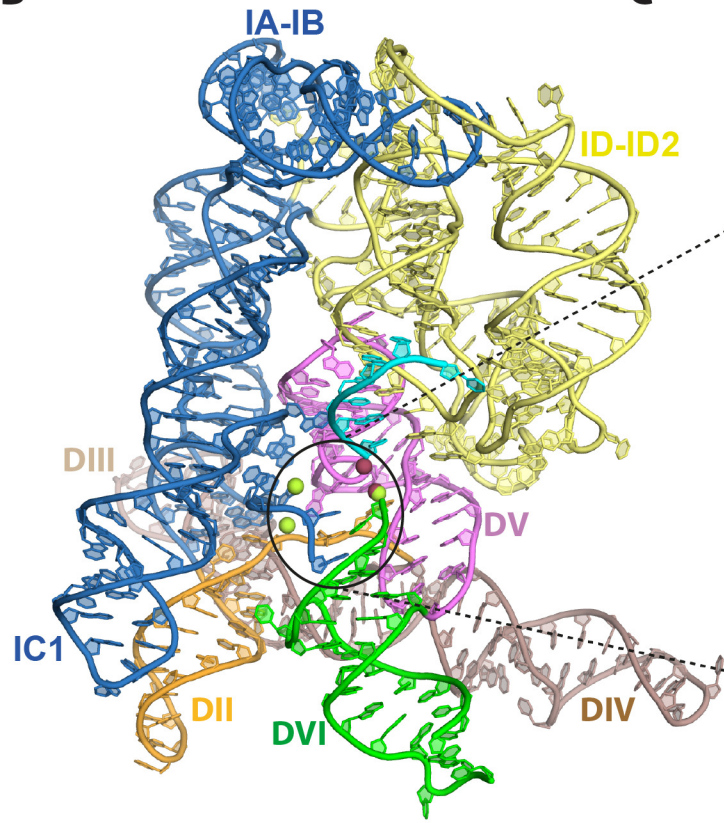






A**B****C**

A

B**C**